

<https://doi.org/10.1038/s42004-024-01335-8>

Light-induced rolling of azobenzene polymer thin films for wrapping subcellular neuronal structures

Check for updates

Marta J. I. Airaghi Leccardi¹, Benoît X. E. Desbiolles¹, Anna Y. Haddad¹, Baju C. Joy¹, Chen Song² & Deblina Sarkar¹ ✉

Neurons are essential cells composing our nervous system and orchestrating our body, thoughts, and emotions. Recently, research efforts have been focused on studying not only their collective structure and functions but also the single-cell properties as an individual complex system. Nanoscale technology has the potential to unravel mysteries in neuroscience and provide support to the neuron by measuring and influencing several aspects of the cell. As wearable devices interact with different parts of our body, we could envision a thousand times smaller interface to conform on and around subcellular regions of the neurons for unprecedented contact, probing, and control. However, a major challenge is to develop an interface that can morph to the extreme curvatures of subcellular structures. Here, we address this challenge with the development of a platform that conforms even to small neuronal processes. To achieve this, we produced a wireless platform made of an azobenzene polymer that undergoes on-demand light-induced folding with sub-micrometer radius of curvature. We show that these platforms can be fabricated with an adjustable form factor, micro-injected onto neuronal cultures, and can delicately wrap various morphologies of neuronal processes in vitro, toward obtaining seamless biointerfaces with an increased coupling with the cell membrane. Our in vitro testings did not show any adverse effects of the platforms in contact with the neurons. Additionally, for future functionality, nanoparticles or optoelectronic materials could be blended with the azobenzene polymer, and 2D materials on the platform surface could be safely folded to the high curvatures without mechanical failure, as per our calculations. Ultimately, this technology could lay the foundation for future integration of wirelessly actuated materials within or on its platform for neuromodulation, recording, and neuroprotection at the subcellular level.

For centuries, cells have been considered the biological building blocks of our organs and tissues. As such, they are often presumed to behave like a fundamental unit. However, predominantly in neuroscience, cells have been demonstrated to have a particular polarity¹. For instance, certain activities only happen in specific subcellular compartments, trafficking moves in precise directions, and membrane proteins are heterogeneously distributed on the cell surface^{1–6}. Similar to the human body and its task-specialized components such as legs, hands, eyes, nerves, and bones, neurons have axons, somas, dendrites, microtubules, or axonal initial segments where dedicated cellular processes occur. Therefore, probing and modulating subcellular regions of neurons can lead to discovering

significant breakthroughs and to controlling cellular behaviors at unprecedented levels^{7–10}.

Combining advanced technology with biology is thus of particular interest^{9–12}. Not only does technology offer countless versatile ways to interrogate and control various aspects of the cell's activities, but it could also provide enhanced functionalities to the cell that are not achievable from the biological repertoire¹³. We could envision a new type of biomedical device interacting with a single neuron through a wireless biointerface. Supplied with cutting-edge nanotransducers or blended with functional materials, the electrical and metabolic activity of neurons could be measured and/or modulated with subcellular resolution or restored, for example by

¹MIT Media Lab, Massachusetts Institute of Technology, Cambridge, MA, USA. ²Department of Chemical Engineering, Massachusetts Institute of Technology, Cambridge, MA, USA. ✉ e-mail: deblina@mit.edu

developing myelin-like layers to reduce axonal degeneration in demyelinating diseases such as multiple sclerosis¹⁴.

One of the major challenges in developing this type of technology for neurons lies in creating a seamless neural interface to uniquely connect with the cell. More specifically, the freestanding device should have an adaptable form factor (2–50 μm by 2–50 μm by 0.01–0.5 μm) and delicately conform to any cell shape, including wrapping around high-curvature structures like neuronal processes, which in the brain have a diameter between 150 nm and 5 μm ¹⁵. This would allow the devices and their functional parts to intimately contact the membrane, obtaining a superior transduction efficiency with the technology and an ideal symbiosis with the cell thanks to the reduced geometrical and mechanical mismatch with the cellular environment^{12,16,17}. To date, developing a cell-conformable substrate remains an unmet challenge.

Here, we tackle this quest by developing a thin freestanding platform able to actively and conformably enfold neuronal structures and wrap around neuronal processes like axons and dendrites (Fig. 1). These platforms would be dispersed in physiological solution and microinjected into the nervous tissue (Fig. 1A and B). Then, once in contact with the cells, they could be triggered by an external stimulus to fold and develop around the cellular parts (Fig. 1C and D). Ideally, these structures can morph according to the shape of the subcellular region they interface.

Due to their high curvature, axons and dendrites are among the most difficult neuronal structures to conformally enwrap with a synthetic platform. Hence, in this paper, we focus on a technology able to achieve wrapping of neuronal processes, and one of the most versatile materials for this purpose is azobenzene-containing polymers. Azobenzene polymers possess azobenzene units in their chain or side groups, which undergo *trans-cis* isomerization upon illumination, usually resulting in an overall photoinduced motion of the polymeric layer^{18–20}. Here, we evaluate an azobenzene polymer, poly(disperse red 1 methacrylate) (pDR1M, Supplementary Fig. 1A), as a potential thin-film platform for on-demand folding and wrapping of neuronal processes. To induce rolling, we use green light at 545–555 nm, and we demonstrate that linear polarization of the light can be used to control the folding direction of the films. Additionally, we hypothesize how rolling of the homogeneous pDR1M film is achieved and the possible molecular mechanisms behind its driving force. Then, we show that pDR1M thin platforms can actively wrap artificial axon-like fibers and neuronal processes *in vitro* without causing neuronal death or damage. Remarkably, a single platform can conform to varying curvatures and shapes, enfolding even geometrically complex regions of the neurons. Finally, to engage in the feasibility of integrating additional technologies and advanced functionalities on these platforms, we calculate that several functional materials (particularly two-dimensional nanomaterials) can sustain exceptionally high bending curvature as required for the polymeric platform wrapped around fibers of $\leq 1 \mu\text{m}$ diameter.

Results

The required number of devices for brain-machine interfaces with sub-cellular resolution on millions of neurons could get very high. Additionally, these devices should be injected through a minimal volume. Consequently, the first challenge comprised manufacturing numerous sub-10 μm , free-standing, and thin polymeric structures that are inconveniently susceptible to standard photolithographic processes and chemicals. Moreover, these structures should ideally be harvested in cell-compatible solutions with minimal solvent exchange steps to avoid losses in the process. Hence, we developed a fabrication method to obtain at least 8000 devices per μL of physiological solution or cell media (Fig. 2A). Briefly, we used soft lithography with a polydimethylsiloxane (PDMS) stamp to mold the liquid polymer dispersion onto a sacrificial layer of dextran (Fig. 2A-i) and obtain millions of pDR1M structures of about 250 nm in thickness over 1 cm^2 of area (Fig. 2A-ii). Of course, the exact number of structures depends on their size: for instance, over 1,234,000 squares of 6 μm by 6 μm can be produced per cm^2 . Once the PDMS molds and the polymer solutions are prepared, the expeditious 6 minutes long stamping procedure can be repeated several times. Afterward, a baking step is performed to ensure all solvents are evaporated. Once the structures are patterned on the dextran layer, an oxygen plasma etching guarantees that residual pDR1M is removed between the structures that will ultimately be 150 nm thick (Fig. 2A-iii). In this step, the dextran release layer is also etched between the pDR1M arrangements, eventually reducing its concentration in the releasing medium. Lastly, the dextran layer is dissolved in aqueous solutions such as cell media, and the pDR1M structures are released from the substrate and collected without solvent exchange or rinsing necessary since dextran is a biocompatible polysaccharide (Fig. 2A-iv). Figure 2B-i and ii depict examples of produced pDR1M structures, where various shapes can be patterned on the release layer with remarkable reliability. Moreover, the scanning electron microscopy (SEM) images illustrate that the dextran layer is etched around the structures. Figure 2B-iii shows 6 μm by 6 μm pDR1M squares being released from the substrate once immersed in water. Conveniently, pDR1M has a broad absorption in the 420–550 nm range (Supplementary Fig. 1B) and autofluorescence in the red, making it possible to visualize with fluorescent microscopy such as confocal microscopes (Fig. 2B-ii and C-iii).

Then, we observed the effect of illumination on the shape changes of the pDR1M structures. Using a fluorescent microscope with excitation light filtered at $545 \pm 30 \text{ nm}$, it was possible to consistently induce the rolling of squared and rectangular thin platforms dispersed in aqueous solutions (Fig. 2C). As visible in Fig. 2C-i, all the structures in the briefly irradiated region underwent photoinduced folding as opposed to those not irradiated. It is important to notice that the rolled structures maintain their shape once the illumination stops, even after several days in liquid or air. SEM and confocal images were used to observe the three-dimensional (3D) structure of the rolled-up pDR1M layers (Fig. 2C-ii and iii, Supplementary Fig. 3B and

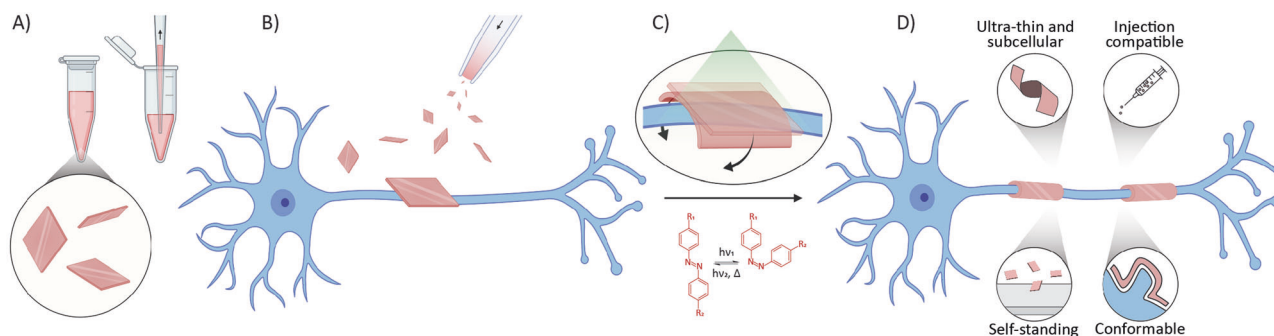


Fig. 1 | Cell-conformable platforms. **A** Generalized freestanding thin-film micro-devices of 5–100 μm^2 dispersed in physiological solution or cell medium at high concentrations. **B** Microinjection of the devices into cultures, tissues, or organs. **C** Devices engineered to roll can actively wrap cellular parts like neuronal processes

through a wireless stimulus. For instance, materials containing azobenzene units can transform when illuminated thanks to the photoinduced isomerization of azo-benzenes. **D** Illustrative placement and characteristics of the developed technology. Illustrations partially created with BioRender.com.

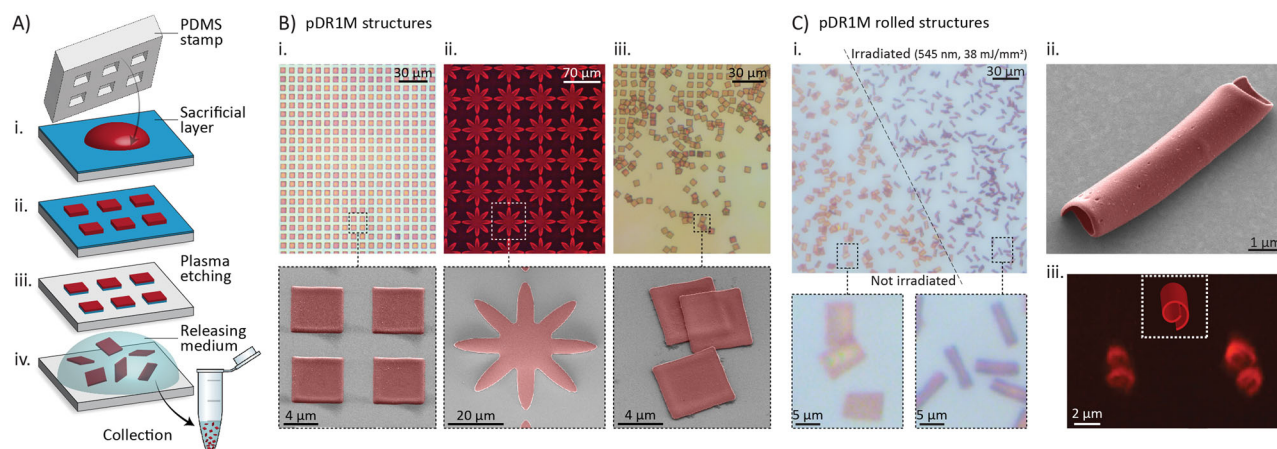


Fig. 2 | Fabrication, harvesting, and photoinduced rolling of pDR1M thin platforms. **A** Manufacturing process: a drop of polymer solution is molded thanks to a PDMS stamp onto a substrate coated with a sacrificial layer (i, ii); then, after a short oxygen plasma etching, the patterned structures are released from the substrate through sacrificial layer dissolution and collected (iii, iv). **B** pDR1M structures of various sizes and shapes, before (i, ii) and after releasing (iii). The top line shows optical microscopy images (fluorescent imaging with excitation/emission at 545/620 nm), while colored SEM images are depicted at the bottom. **C** Light-induced

rolling of the fabricated pDR1M platforms: an optical image of irradiated and not irradiated $6 \mu\text{m}$ by $9 \mu\text{m}$ rectangles in water (i), a colored SEM image of a rolled $6 \mu\text{m}$ by $6 \mu\text{m}$ structure after drying (ii), and a confocal microscopy image of two rolled $6 \mu\text{m}$ by $6 \mu\text{m}$ structures in water (iii, excitation/emission at 561/615 nm), where a representation of the microtubes orientation is illustrated in the white dotted inset. The pDR1M platforms were rolled using fluorescent light filtered at 545 nm for 3 (12.5 mW mm^{-2}).

C), demonstrating that microtubes are formed with an internal diameter between 0.5 and $2 \mu\text{m}$, which is ideal for wrapping neural processes. Remarkably, microtubes of these dimensions are produced on demand from polymeric freestanding platforms for the first time.

Once established that the formed structures are microtubes potentially able to accommodate an axon, we asked whether we could control the folding direction to facilitate the wrapping of fibers oriented in specific ways. This is particularly helpful for future applications in the peripheral and central nervous systems involving nerve bundles and neurons with oriented axons, which is the case for most regions of the brain²¹.

According to various studies^{19,20,22,23}, the photoisomerization of azobenzene moieties depends on the linear polarization orientation of the light with respect to the orientation of their dipole moment in the *trans* state, which leads to a potential polarization-dependent folding direction of the overall polymeric layer. Therefore, we analyzed the response of the freestanding pDR1M platforms to linearly polarized green light at 545 nm and compared it to the unpolarized one (Fig. 3A and B). For these experiments, we investigated two geometries of the thin layers, namely squares of $6 \mu\text{m}$ by $6 \mu\text{m}$ (aspect ratio 1:1) and rectangles of $6 \mu\text{m}$ by $9 \mu\text{m}$ (aspect ratio 2:3). Indeed, the linear polarization of the light greatly affected the in-plane orientation of the rolling axis for both geometries. As illustrated by the optical images in Fig. 3A, the microtubes develop along the axis parallel to the polarization direction. To obtain quantitative data, we computed the occurrence of microtubes formation in specific directions depending on the geometry of the platforms (aspect ratio), their initial orientation, and the light linear polarization direction (Fig. 3B). In the case of unpolarized light, squared structures seem to roll in random orientations, while rectangles tend to form microtubes along their long axis. However, an evident preferential rolling direction parallel to the light polarization direction can be enforced for both geometries independently from their initial orientation. This demonstrates a shape- and polarization-dependent folding orientation valuable for the versatile remote control of axonal wrapping.

In addition to the abovementioned observations, we evaluated how the folding process is achieved. Specifically, we looked at the shape changes of pDR1M platforms at different time points during illumination. The optical microscope snapshots in Fig. 3C-i and Supplementary Fig. 2 show that the platforms are first subjected to a slight in-plane elongation when illuminated with linearly polarized light. The elongation is in the polarization direction and seems to initiate the folding and direct the rolling process. Even though

it was not visible in complex geometries like flower-like shapes (Supplementary Fig. 2), this strain appeared evident for squared, rectangular, and even round shapes. Moreover, we could capture SEM images of $6 \mu\text{m}$ by $6 \mu\text{m}$ platforms stopped at different stages of rolling depending on the delivered energy of the linearly polarized light (Fig. 3C-ii). These images also show how the layers are eventually stretched – parallelly to the polarization direction—up to 160% of their original length. Remarkably, by adjusting the illumination dose (or time \times intensity) with or without linear polarization, it is possible to control the extent of the rolling, that is, the final diameter of the microtubes. We observed that the diameter could be controlled down to about $0.5 \mu\text{m}$, after which higher light energies result in more elongated or impractically deformed microtubes. Nevertheless, this ability to remotely and gently adjust the final diameter of sub- $10 \mu\text{m}$ structures could be advantageous for biological entities with various sizes and curvatures.

Furthermore, we verified the out-of-plane folding direction, i.e., whether the platforms fold toward the incoming light or away from it, or randomly. Our SEM observations indicate that all the platforms fold in whichever direction makes the side on the top during the fabrication transpire on the outer side of the microtubes (Supplementary Fig. 3A). The SEM images show rougher surfaces, which were the top surfaces after microfabrication, always ending up on the outer side of the microtubes (Fig. 2C-ii and Supplementary Fig. 3B and C). Moreover, platforms top-coated with a thin layer of gold also folded with gold on the outer side (example shown in Supplementary Fig. 3D). Therefore, the out-of-plane folding direction is independent from the incoming light direction. This feature will allow future functional structures coated or patterned on the bottom side of the platforms to consistently end up internally, that is, in contact with the cell membrane. Vice versa, active sites on top of the platforms will go externally, which might be required depending on the application.

Thus, we hypothesized which molecular mechanisms could be responsible for the observed optomechanical reactions of the thin pDR1M films. According to the observations and literature review^{22–24}, we believe three simultaneous processes occur when the platforms are illuminated. The first one is a reorientation and alignment of the azobenzene units according to the Weigert effect (Fig. 3D), where each chromophore undergoes cycles of photoisomerization *trans* \rightarrow *cis* \rightarrow *trans* until its transition moment reorients orthogonal to the linear polarization direction of the light (Fig. 3D-i). At this point, light absorption does not induce reconfiguration to

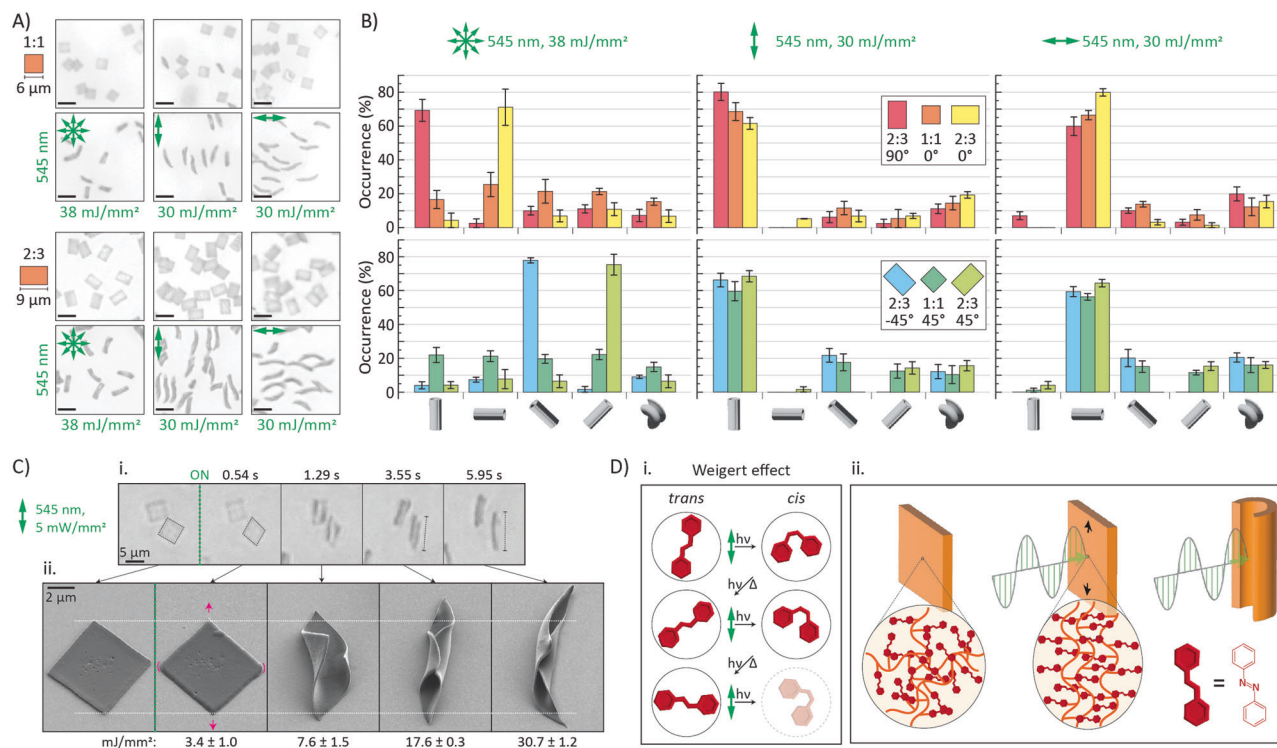


Fig. 3 | Control of pDR1M platforms rolling. **A** Representative optical microscopy images of 6 μm by 6 μm (top six images) and 6 μm by 9 μm (bottom six images) pDR1M platforms dispersed in water before and after illumination with light characteristics described in green (left: no polarization, middle: vertical polarization, right: horizontal polarization). The alignment of the microtubes along the polarization direction is clearly visible; moreover, it can be noticed that rectangles irradiated without polarization rolled along their long side. Scale bars: 10 μm . **B** Analysis of rolling direction: occurrence of microtubes formation along specific directions (shown on the x-axis) depending on the sheets' aspect ratio and initial orientation (depicted in the legend) and light polarization (shown at the top). The data also includes structures that formed undefined shapes (as fifth column). The columns represent the mean \pm s.e.m. of three samples (each sample including

20–40 structures per condition). The micrographs in (A) show a representative area of the analyzed images. **C** Snapshots during microtubes formation of pDR1M 6 μm -wide squares responding to the depicted light stimulus. An elongation along the polarization direction occurs prior rolling and continues even after the microtube is formed. At the bottom, SEM images, taken with a tilt angle of 30°, show dried samples found at the corresponding rolling stage. **D** Hypothesized molecular mechanisms responsible for pDR1M deformation and rolling: the Weigert effect, in which the azobenzene units reorient perpendicular to the linear polarization direction (i), could cause reorganization of the polymer molecules and elongation along the light polarization direction (ii). This elongation, together with releasing fabrication stresses thanks to photofluidization, could induce the rolling.

cis isomer anymore, and the large fraction of azobenzene units oriented anisotropically generate a directional strain of the pDR1M layer (Fig. 3D-ii). The second and third processes justify the independence of the out-of-plane folding direction from the incoming light path as following: In one case, a substrate- and molding-dependent anisotropy of the molecular organization during fabrication is postulated^{25,26}. Consequently, this organization could result in one side of the platform undergoing photo-mechanical transformation differently than the other²⁷. In the other case, due to the fast isomeric cycling, a photofluidization of the material might occur during illumination, with or without polarization²⁸. This temporary and reversible liquefaction-like process could reduce the stiffness of the polymer and allow not only the polarization-dependent photo-reorientation of the pDR1M molecules but also the release of any internal stresses built during fabrication. Once the light is removed, the material might recover its original stiffness, “petrifying” the platform into its new shape. However, additional specialized characterizations will be needed to confirm our hypotheses.

Then, we evaluated the capabilities of the pDR1M platforms to wrap in water synthetic fibers made of electrospun polyacrylonitrile (PAN). A stimulus of light polarized parallel with the PAN fibers helps the randomly distributed platforms to successfully wrap the 1 to 3 μm wide fibers (Fig. 4A and B). Note that, to fully wrap around the circumference, the fibers need to be suspended away from the substrate and possess the third dimensionality. Figure 4B shows SEM images of exemplary pDR1M structures wrapped around various fiber diameters and even multiple fibers simultaneously. The conformability of these layers around various curvatures encourages the

photofluidization hypothesis and active rolling mechanisms during illumination. Note that the proposed rolling mechanism leading to unidirectional folding is applied to the out-of-plane folding direction without other types of constraints. However, other constraints could affect the folding dynamics. For example, in Fig. 4B one can notice that in the presence of fibers, sections of some platforms seem to fold in both out-of-plane directions. This is likely due to the fibers being “in the way” of the platforms rolling (or being wrapped), and a more complex mechanics could take place due to the material not being able to freely move. Hence, with photofluidization increasing the softness of the material during illumination, it is possible that other constraints against the rolling intentions will make the material bend in a different manner. Moreover, to confirm that wrapping is not due to capillary forces during water evaporation for SEM sample preparation, we imaged not illuminated platforms on fibers revealing flat, cracked, and suspended structures as a demonstration of their relatively high stiffness and impossibility to fold at such high curvatures without molecular reorientation and/or photofluidization (Supplementary Fig. 4A and B). Additionally, we estimated that the bending stress of a 150 nm pDR1M layer would reach its maximum tensile strength and induce cracking when folded with a diameter of about 6 μm (assuming a Young's modulus of 1 GPa, Poisson's ratio of 0.4, and ultimate tensile strength of 30 MPa^{29,30}), which is one order of magnitude larger than the demonstrated photoinduced diameters (Fig. 2C and Supplementary Fig. 3B and C).

Indeed, for future applications, the potential transducers and other coated layers on the rolling platforms also need to sustain and operate at

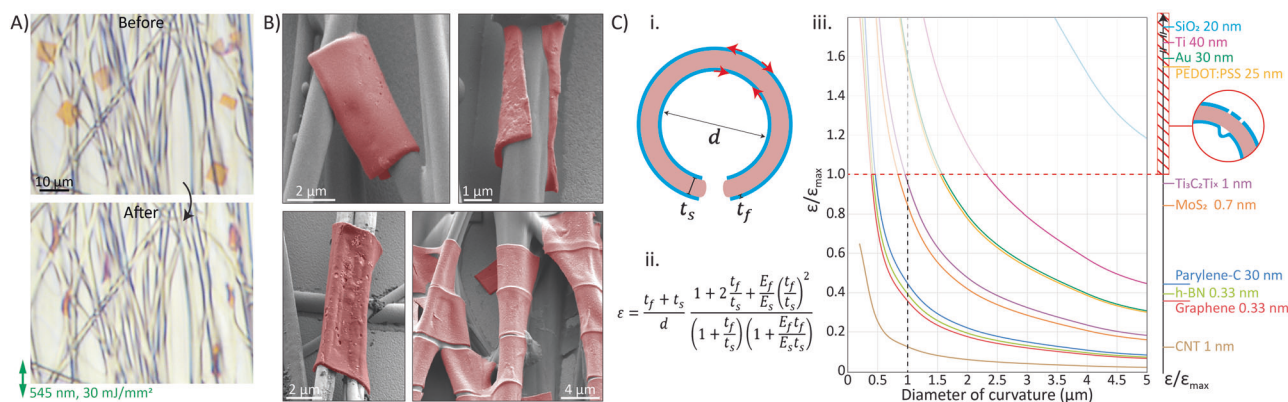


Fig. 4 | Wrapping of artificial fibers and theoretical bending strains on various materials. **A** Optical micrographs of several pDRIM platforms dispersed on PAN electrospun fibers in water and rolled with the depicted light stimulus. **B** Colored SEM images of dried PAN fibers with rolled pDRIM platforms. **C** i Bending strains endured by the thin films (represented in blue) coated on either side of the rolling platforms. ii and iii, Evolution of the tensile strain (ϵ , as calculated in ii, also described as Eq. (2) in the Materials and Methods section) normalized to the material's

ultimate strain (ϵ_{\max}) with the diameter of the microtubes. The black solid vertical line on the right side of the graph represents the values of ϵ/ϵ_{\max} at 1 μm rolling diameter (vertical black dotted line) for the various materials. The thin films fail above $\epsilon/\epsilon_{\max} = 1$ (horizontal red dotted line). d : microtube diameter, t_s : substrate (pDRIM) thickness, t_f : film thickness, E_s : substrate Young's modulus, E_f : film Young's modulus. All parameters are defined in Table 1 in the "Materials and Methods" section.

extremely high curvatures without failure. Therefore, we analyzed the calculated evolution of the strain for various electronic materials deposited on the platform rolling up to 0.2 μm in diameter (Fig. 4C). Films ensuing inside the microtubes would mainly undergo compressive strain, while those outside would be subjected to tensile strain as described in Fig. 4C-i and ii. The resulting tensile strain normalized to the ultimate tensile strain for each material is plotted in Fig. 4C-iii. Above $\epsilon/\epsilon_{\max} = 1$, failure mechanisms such as cracking and buckling occur at the thin films³¹, happening at curvatures higher than 1.5 μm in diameter for several conventional electronic materials like Au, Ti, SiO₂, and poly(3,4-ethylenedioxythiophene):poly(styrenesulfonate) (PEDOT:PSS). However, as depicted, 2D materials, nanomaterials, and soft polymers or elastomers could fold below 1 μm in diameter without failing. This result is not surprising as several 2D and nanomaterials are known to endure intense mechanical deformations^{32–34}. Here, we have shown calculations for representative and conventional semiconducting, insulating, and metallic 2D materials. However, it is important to highlight that the functionality of the platform is not limited to layers patterned on top of it: Blending the pDRIM with nanoparticles or other polymers - such as optoelectronic materials like Poly(3-hexylthiophene-2,5-diyl) (P3HT, often used for wireless neuromodulation^{35–37}) - can give the platforms the capability of transducing electromagnetic waves into charges that stimulate the cells^{35–38} and, vice versa, membrane potential into electromagnetic waves (disturbances) that can be read wirelessly^{39,40}. We tested that blending P3HT with pDRIM at a ratio of 1:3 did not seem to impede the rolling process (Supplementary Fig. 3E–G). Moreover, an insulating film such as pDRIM by itself wrapped around cell bodies or processes could still have a function in affecting the membrane capacitance. Although future work will be required to test such a feature, we can foresee how this could be relevant in studies involving, for instance, the myelin function.

Finally, we investigated whether the pDRIM platforms can wrap neuronal processes in vitro. The platforms were delivered to 2D cultures of live primary rat neurons and left to sediment for at least one day, randomly depositing on several processes, somas, and the substrate (Fig. 5A). Then, the rolling of the platforms and potential wrapping were induced by illuminating the cells without polarization due to the random organization of the processes (Fig. 5A and B). SEM imaging of the neurons was performed to better evaluate the pDRIM wrapping, and representative images are shown in Fig. 5C and Supplementary Fig. 5. Since the cells in 2D cultures adhere well to the substrate, it is difficult for the platforms to wrap the processes entirely (see examples in Supplementary Fig. 5A–E). However, some

platforms could be found below (Supplementary Fig. 5F and G) or on suspended processes (Fig. 5C and Supplementary Fig. 5H), leading to a more efficient wrapping and demonstrating for the first time that it is possible to wrap neuronal processes such as axons and dendrites with synthetic materials and on demand. Interestingly, the plausible softening of the pDRIM platform thanks to photofluidization allows for a conformable wrapping of a single platform on various cellular structures and curvatures. As visible in Fig. 5C on the right, the pDRIM layer is able to gently envelop part of the soma and a couple of sub-0.5 μm processes without apparently damaging them. It is also important to note that, intrinsic to in vitro culture where glass is present and provides physical constraints, the platforms could "stick" to it making it more difficult to roll. This phenomenon can only happen in vitro and is not expected to be an issue in 3D or in vivo. In fact, the demonstration that our platforms are able to roll even in the presence of the physical constraints of the glass substrate is very promising and shows how strong this photo-mechanical effect can be, especially with micro-scaled and thin films (6 $\mu\text{m} \times 6 \mu\text{m} \times 150\text{--}200 \text{ nm}$).

To verify that the presence of the platforms, as well as the illumination and rolling processes, do not affect the function, structure, and viability of the cultured neurons, we performed 3-[4,5-dimethylthiazol-2-yl]-2,5-diphenyl-tetrazolium bromide (MTT) assays, patch-clamping, imaging with a live cells indicator, and immunocytochemistry detection of the cytoskeleton protein α -tubulin (Fig. 5D and Supplementary Fig. 6). As depicted in Fig. 5D-i, the MTT assay resulted in very similar metabolic activity (represented as absorbance values) among the 16-days old control group and the 16-days old cells incubated with 6 μm by 6 μm pDRIM platforms at 953 \pm 109 per mm² for 4, 6, and 9 days (2, 4, and 7 days after illumination), depicted in the image as 4(2), 6(4), and 9(7) respectively. Additionally, we included the absorbance values for platforms that were not illuminated (9 days-flat) and for double the concentration of platforms with respect to the other conditions (9(7)-2x, 1889 \pm 222 per mm²), also showing no significant differences in metabolic activity. The viability values calculated from the absorbances were 102% \pm 25%, 107% \pm 27%, 112% \pm 29%, 89% \pm 23%, and 97% \pm 24% for 4, 6, 9 days, 9 flat, and 9 days 2x, respectively. As a supplementary viability test, we performed imaging of a 37-day-old neuronal culture incubated for 27 days (26 days after illumination) with 6 μm by 6 μm pDRIM platforms, showing >86% of cells still alive (Fig. 5D-ii), which is similar to control cells cultured without the platforms. Moreover, excitability and resting potential of neurons cultured with and without the rolled platforms show no significant differences (Supplementary Fig. 6A and B) as does the cytoskeleton (microtubules) integrity imaged

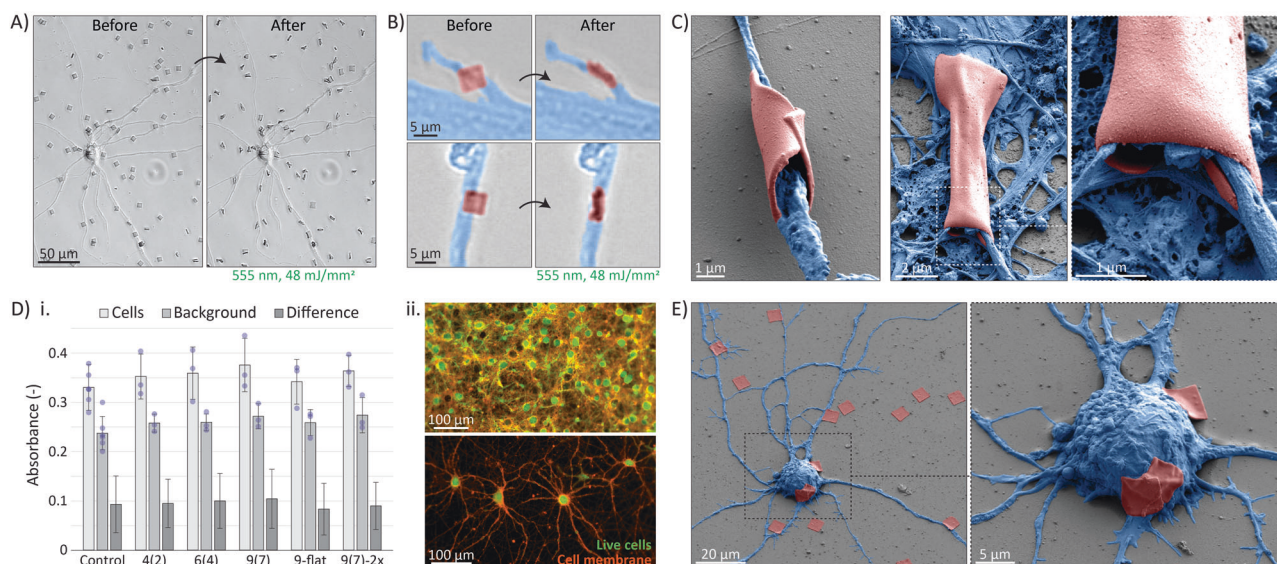


Fig. 5 | Wrapping of neuronal processes in vitro. **A** Exemplary optical images of cultured rat hippocampal neurons and $6\ \mu\text{m}$ by $6\ \mu\text{m}$ pDR1M platforms before and after rolling with the depicted light stimulus (no polarization, $8\ \text{mW}\ \text{mm}^{-2}$, 6 s).

B Exemplary colored optical images at higher magnification of the neurons (blue) and $6\ \mu\text{m}$ by $6\ \mu\text{m}$ pDR1M platforms (red) before and after rolling with the depicted light stimulus (no polarization, $8\ \text{mW}\ \text{mm}^{-2}$, 6 s). **C** Colored SEM images of neurons (blue) with the pDR1M wrapped structures (red). The images on the right show how the layer can conform to various curvatures and even delicately wrap sub- $0.5\ \mu\text{m}$ processes, as revealed in the magnified inset. **D** Biocompatibility tests of 16-day-old hippocampal rat neurons cultured with the pDR1M platforms. (i) MTT assays—Control: cells without platforms, 4(2): cells incubated with the platforms for 4 days (2 days post-illumination), 6(4): cells incubated with the platforms for 6 days (4 days post-illumination), 9(7): cells incubated with the platforms for 9 days (7 days post-

illumination), 9-flat: cells incubated with the platforms for 9 days and without illumination, 9(7)-2x: cells incubated with double the concentration of the platforms (1889 ± 222 per mm^2 instead of 953 ± 109 per mm^2) for 9 days (7 days post-illumination). All absorbance values display the mean \pm standard deviation of at least three replicas for each condition. The background values are obtained from the cell media supplemented with the platforms, while the difference (=cells – background) represents the amount of absorbance due to the metabolic activity of the cells. (ii) Viability imaging overview of a 37-day-old rat hippocampal neurons cultured for 27 days (26 days after illumination) with the pDR1M platforms. Top: a dense region, bottom: sparse neurons. Green: live cells stained with a cell viability indicator (FITC filter set), red: cell membrane stain (TRITC filter set). **E** Colored SEM images of a neuron (blue) with several $6\ \mu\text{m}$ by $6\ \mu\text{m}$ pDR1M platforms (red).

by the immunostaining (Supplementary Fig. 6C and Supplementary Video 1 showing α -tubulin immunostaining with platforms rolled around a neurite). Therefore, we could conclude that neither the presence of the platforms, even at high density nor the illumination and rolling processes seem to be harmful to cultured neurons, particularly as there is no negative trend the longer the neurons interact with the platforms (Fig. 5D-i). Indeed, it remains to investigate other phenotypic aspects of the cells interacting with the platforms, such as gene expression and axonal transport. However, the neurons being delicate cells and able to assemble and disassemble processes through remodeling, they would have been adversely affected by the platforms by undergoing either cell death or partial degeneration of wrapped processes⁴¹, which should have been visible in the experiments and imaging performed.

In general, these devices might also need to conform to the cell body instead of its processes. As shown in Fig. 5E, the pDR1M platforms are able to conform to lower curvature cell bodies after three days of incubation even without being illuminated, leading to somatic interfaces. In this case, the polymeric nature of the platform, together with the relatively long interaction time with the cells, could have allowed good conformability even of several non-illuminated platforms. However, for features with higher curvature, light-induced folding is required.

Generally, the neurons seem to interact positively with the pDR1M layer—either flat or rolled—by sensing its presence, form, and material through their micro processes, even passing them through the nanoscopic holes on the platforms (Supplementary Fig. 5I-K). On that note, these holes likely appear during patterning of pDR1M due to fast polymer solvent evaporation, and although they could be seen as manufacturing defects, they could be in fact beneficial for facilitating the diffusion of metabolites and other biomolecules through the membrane-interfacing platforms.

Discussion

We introduced the concept of a versatile and injectable platform able to actively and conformably enwrap most structures of the neurons down to a radius of curvature of $250\ \text{nm}$. The wrapping of neurites, such as axons and dendrites, with the platform could lead to a stable and proximate bio-interface compatible with thin-film-based nanoengineered technology.

As a step toward achieving this goal, we proposed pDR1M as substrate material for on-demand photoinduced rolling of freestanding layers thanks to the comprised azobenzene moieties. First, we demonstrated that we could achieve controlled rolling extent and direction, and we suggested possible molecular mechanisms involved in the process. Then, we showed that it is possible to achieve conformable wrapping of thin sub- $10\ \mu\text{m}$ pDR1M platforms around artificial fibers and neuronal processes in vitro. This can be a promising tool for neuroscience, especially if conjugated with biomolecules or combined with other functional nanomaterials or soft matter for wireless modalities.

It is important to note that, although the photo-mechanical phenomenon of azobenzene-based materials is well known, light-induced rolling of freestanding micron-scale polymeric thin films was not previously reported, particularly with such small diameters. The reported polymeric structures able to fold or roll on-demand found in literature are mm-scale and some of them are also surface-bound (not freestanding)²⁰. Hence, apart from the first demonstration of rolling around neurons, this work also reports the first demonstration of freestanding thin films able to form microtubules with sub- μm diameters on demand with light and controlled orientation.

The main advantage of freestanding and subcellular devices is that their injected number and density can be adjusted to the needs: Theoretically, we could inject as many as 100 s of thousands or as little as one. The platforms are meant to facilitate future wireless communication with and modulation

of neurons with high resolution by employing, for example, patterned light used for optogenetics⁴². The idea is to equip most cells in the targeted region with a device—a transducer—that is available at will for interactions with possibly individual cells, by employing high-resolution patterned wireless control. Thus, using our technology, scalability to a large number of neurons is possible while simultaneously achieving high resolution. In contrast, low resolution wrapping implants such as nerve bundles cuff electrodes lose the ability to target individual inner cells⁴³. Moreover, the reduced size of the devices compared to conventional implants has the advantages of reducing invasiveness (devices could move with the brain micromotion more easily, and therefore lowering the risk of fibrotic reaction) and better device-cell interface.

Future work can include integrating and testing functional materials that could enable neurologically relevant applications. For instance, optoelectronic polymers or nanomaterials could be deposited on the platform or mixed with pDR1M to achieve wireless electrical neuromodulation or electrophysiological sensing^{40,44–46}. Our preliminary work shows that rolling of the platforms can still be achieved when pDR1M is blended with P3HT (an optoelectronic material often used for wireless neuromodulation^{35–37}). Thanks to the wrapping, the proximity and surface area of the material in contact with the neuronal membrane can be increased, increasing the sealing resistance and allowing for better electrical^{47,48}, thermal⁴⁹, chemical^{50,51}, and mechanical⁵² coupling with the cell. Not only could these interfaces provide modulation, sensing, and drug delivery, but they could also be engineered to electrically and periodically insulate the axons and induce nodal ion channel clustering to obtain a synthetic myelin-like layer to study neurodegeneration dynamics and potential neuroprotection in demyelinating diseases.

Moreover, other aspects of the technology could be enhanced. One is to place the pDR1M layer specifically onto neurons (increasing targeting and wrapping yield) or even on precise subcellular parts of neurons, like their axons or axonal initial segments, avoiding non-specific interactions or rolling of several platforms without wrapping neurites. For that, functionalization strategies could be applied, where molecules complementary to neuronal and axonal membrane proteins are attached to the platforms, which will then specifically bind to the targeted subcellular region⁵³.

Future work can also focus on implementation of this technology in vivo. Our preliminary injection and rolling experiments (Supplementary Note 1) performed in brain tissue phantoms (agarose gel 0.6%) show that a volume of about 1.5–1.8 mm³ can be covered with the platforms injected with 5 μ L of suspension in PBS (Supplementary Fig. 7A) and that some of these platforms could roll upon illumination (Supplementary Fig. 7B). These experiments point towards the feasibility of this technology in brain like medium. However, the diffusion and rolling of the platforms in 3D neural tissue and in animals (such as rodents) should be investigated in the future. Moreover, for in vivo applications and actuating the platforms inside the brain, light can be delivered in the brain through different approaches as described in Supplementary Note 2.

Further consideration should also be made about the degradability of the proposed platforms. Although we have not characterized the long-term fate of pDR1M-based platforms, we do not expect the material to degrade quickly inside the body (that is, not before ~1 year) due to its similarity to polymethyl methacrylate (PMMA), which is used as biomedical material with very slow biodegradability^{54,55}. However, thanks to the advancements in materials science and transient devices, options could be explored for tuning the longevity of the platforms based on the applications and allow their degradation into physiologically and environmentally safe byproducts after the required application period is over, to avoid the need for explanation or extraction of the devices. Regarding potential opening of the rolled platform with time, we have not seen any re-expansion (tested for up to 1 month in medium at 37 °C). The platforms are not expected to re-expand even during the degradation of the material, since we do not believe they undergo isomerization if not illuminated, thus locking the new rolled shape in place. These shapes are generally stable under normal conditions until another light stimulus is applied or environmental conditions change

significantly. Studies indicate that the stability of these forms are reliant on the light-induced isomerization and the inherent properties of the polymer structure, rather than on chemical degradation processes, which suggests a robust ability to retain programmed shapes under a variety of conditions that do not involve significant light exposure^{20,56}.

Finally, one could envision communication with devices through other wireless modalities than light, such as magnetic or acoustic waves. These modalities offer a deeper penetration through biological tissues and, therefore, a wider variety of applications including deep-brain stimulation^{11,57}. The platforms could in the future be designed to respond to these fields tuned for rolling, and the nanotechnology on the platform tuned for modulation, sensing, or drug release.

In conclusion, advanced neural interfaces that offer the possibility of interacting with single cells at an unprecedented level can open up new avenues in neuroscience research. Since cells are small and based on soft matter, these interfaces could thrive thanks to the recent technological and manufacturing upsurge of unconventional materials like stimuli-responsive soft materials^{58,59}, organic transducers⁶⁰, and nanomaterials⁶¹, which are more suited to interact with biological entities compared to traditional bulky, inorganic structures. Thus, the proposed technology could bring us a little closer to advancing the symbiosis of neural interfaces with biological material.

Materials and methods

Fabrication and harvesting of pDR1M structures

Materials. Silicon/Silicon dioxide wafers (Si/SiO₂ wafers, thermal oxide 285 nm, 4", p-type, Graphene Supermarket, cat# W-P-300-1P), AZ 3312 photoresist (Integrated Micro Materials), Hexamethyldisilazane (HMDS, 100%, Transene, cat# 100-HMDS100), AZ 300MIF developer (metal ion free industry standard 0.261 N and 2.38 wt% Tetra Methyl Ammonium Hydroxide, Integrated Micro Materials), Buffered Oxide Etchant (BOE 7:1, 35% Ammonium Fluoride and 6.2% Hydrofluoric Acid in water, KMG Chemicals, cat# 408-062058), Acetone (ACS reagent, $\geq 99.5\%$, Sigma-Aldrich, cat# 179124), Isopropyl Alcohol (IPA, $\geq 99.5\%$, ACS certified, Fisher Scientific, cat# A416-20), Polydimethylsiloxane (PDMS, SYLGARD™ 184 Silicone Elastomer Base and Curing Agent, Dow, cat# 2646340), Silicon wafers (Si wafers, 4", p-type, WaferPro, cat# C04008), Dextran (Dextran 40 from *Leuconostoc* spp., Mw ~40,000 g mol⁻¹, Sigma-Aldrich, cat# 31389), Poly(Disperse Red 1 Methacrylate) (pDR1M, Sigma-Aldrich, cat# 579009), Chloroform (anhydrous, $\geq 99\%$, contains 0.5–1.0% ethanol as stabilizer, Sigma-Aldrich, cat# 288306). All materials were used as received without further purification.

Equipment. Plasma asher (Diener Atto, 13.56 MHz/300 W, Diener Electronic, Ebhausen, Germany), HMDS vacuum vapor prime system (58TA, Yield Engineering Systems, Fremont, CA USA), photoresist spincoater (CEE 200X, Brewer Science, Rolla, MO USA), maskless aligner (MLA 150, Heidelberg Instruments, Heidelberg, Germany), PDMS mixer and degasser (ARE-310, Thinky, Laguna Hills, CA USA), ultrasonic bath (Branson CPX2800H, VWR, cat# 89375-492), spincoater (Laurell WS-650MZ-23NPPB, Laurell Technologies, North Wales, PA USA).

First, the PDMS stamps are fabricated in a class 100/1000 cleanroom facility. Briefly, Si/SiO₂ wafers are oxygen plasma cleaned for 2 min at 200 W, 0.7 mbar, and treated with HMDS for 30 s at 150 °C in a vacuum vapor prime oven before being coated with 1 μ m of AZ 3312 photoresist spincoated at 3000 rpm for 60 s and baked for 70 s at 100 °C. Then, photopatterning is performed at 150 mJ cm⁻² with 375 nm light in a maskless aligner, and the photoresist is baked for 70 s at 110 °C prior to being developed for 70 s with AZ 300MIF and hard-baked for 15 min at 100 °C. Next, the pattern is transferred to the 285 nm thick SiO₂ layer by wet etching in a 7:1 BOE bath for 5:30 min at room temperature. The photoresist is then removed by immersing the wafers in acetone for 2 minutes, rinsing them with IPA, and drying them with a nitrogen gun. Subsequently, the wafers are oxygen plasma treated for 2 minutes at 200 W, 0.7 mbar, and coated with

HMDS for 60 s at 150 °C in the vacuum vapor prime oven before being employed to mold PDMS. For this, the PDMS base and curing agent are mixed at a 10:1 weight ratio and degassed with a mixer and poured onto the patterned Si/SiO₂ wafer. Once the PDMS has been cured for two hours at 65 °C, it is demolded from the wafer and cut into (1.5 cm)² pieces containing the arrays for patterning pDR1M.

Then, the pDR1M is patterned on dextran-coated Si wafer pieces, released in aqueous solutions, and collected for experiments. In detail, dextran solution is prepared by dissolving dextran powder at 50 mg mL⁻¹ in MicroPure water, sonicating for 5 min at low power, and filtering at 0.2 μm with a polyethersulfone (PES) membrane filter. Then, Si wafers are oxygen plasma treated for 2 min at 200 W, 0.7 mbar, spincoated with the dextran solution at 3000 rpm for 60 s, baked on a hotplate for 15 min at 150 °C, and cleaved into (2 cm)² pieces. Next, pDR1M powder is dissolved in chloroform at 1 wt% (15.3 mg mL⁻¹), sonicated for 10 min at low power, and filtered at 0.45 μm with a polytetrafluoroethylene (PTFE) membrane filter. The pDR1M solution is stored at 4 °C, protected from light as much as possible, and re-sonicated before use. Finally, a custom-made molding system, composed of a 10 mL syringe connected to adjustable compressed air and sustained vertically (plunger-down) with a 3D printed support, is used to press a PDMS stamp (self-adhered on the plunger end) onto a dextran-coated Si piece supplied with a 12 μL drop of pDR1M solution. The PDMS stamp is held against the substrate with pDR1M at 18 psi of pressure (controlled by the compressed air regulator) for 5 min, after which the solvent is evaporated through the PDMS stamp, and the stamp is separated from the Si piece leaving the molded pDR1M arrays on the dextran layer. Next, a baking step at 120 °C for 30 min is performed before exposing the structures to oxygen plasma etching for 100 s at 200 W, 0.6 mbar, and releasing them by pipetting up and down 15 μL of water or cell medium directly on the surface of the Si piece. Consequently, the dextran layer gets dissolved, and the pDR1M platforms dispersed in the liquid can be collected with the same pipette and stored in an Eppendorf tube.

Photoinduced rolling and imaging

Materials. CoverWell™ perfusion chambers (Electron Microscopy Sciences, 35 μL, VWR, cat# 100490-788), Indium Tin Oxide substrates (ITO-coated glass slides, Sigma-Aldrich, cat# 703192), linear polarizer (480–550 nm, Ø12.5 mm, Thorlabs, cat# LPVISA050).

Equipment. Upright microscope (ZEISS Axioplan 2 with a FluoArc HBO 100 lamp), scanning electron microscope (SEM, ZEISS Gemini 450, field emission, Inlens and Everhart Thornley Secondary Electron Detectors, Dublin, CA USA), confocal microscope (Nikon ECLIPSE Ti inverted microscope with McBain-Yokogawa and VT-QLC100 spinning disk confocal system, Agilent MLC 400B Dual Fiber Laser, Andor Clara camera for confocal imaging, and Nikon NIS Elements acquisition software).

The micrographs of the fabricated structures were acquired with an upright microscope in fluorescent (ex/em 545/620 nm) or bright-field mode. All the SEM images were obtained with 1.2 kV accelerating voltage, 120 pA probe current, secondary electron (ET) detector, and a 30° tilted view. When applied, image post-processing (brightness/contrast adjustments or coloring) was performed with Adobe Photoshop.

To roll the pDR1M platforms after being released in MicroPure water, 35 μL of the dispersion are injected into a perfusion chamber sealed on an ITO substrate. Then, using an upright microscope, fluorescent light filtered at 545 nm is employed to induce the rolling of the platforms. Bright-field imaging during the rolling process was achieved through a transmitted-light illumination. When necessary, the linear polarizer was fitted and rotated in the microscope compartment for compensators thanks to a homemade slider. The measured light intensity at 545 nm was 15 mW mm⁻² without the polarizer and 5 mW mm⁻² with the polarizer. The structures were illuminated for up to 4 s without polarization and 10 s with polarization, but most structures were rolled after 2.5 s and 6 s, respectively. The rolling direction analyses were obtained by manual counting. After that, the formed

pDR1M microtubes were either imaged in water with a confocal spinning disk microscope (with a 561 nm laser) or let air dry before removing the perfusion chamber and imaging at the SEM as described before.

Synthetic fibers fabrication and wrapping with pDR1M platforms

Materials. Polyacrylonitrile (PAN, Mw ~150,000 g mol⁻¹, Sigma-Aldrich, cat# 181315), N,N-Dimethylformamide (DMF, anhydrous, 99.8%, Sigma-Aldrich, cat# 227056), Polyvinylacetate (PVAc, Mw ~100,000 g mol⁻¹, Sigma-Aldrich, cat# 189480), Acetic acid (ACS reagent, ≥99.7%, Sigma-Aldrich, cat# 695092). All materials were used as received without further purification.

Equipment. Electrospinner (NanoSpinner NS24, Inovenso, Cambridge, MA USA), oven (Thermolyne FD1545M, Thermo Scientific, Waltham, MA USA).

A solution of 14 wt% PAN was prepared by dissolving the polymer in DMF. A solution of 30 wt% PVAc was prepared by dissolving the polymer in a 1:1 water/acetic acid (v/v) mixture. The solutions were stirred until fully dissolved. The fibrous mat on ITO substrates was prepared by transferring aligned fibers produced by electrospinning. First, the ITO substrates were coated with the 30 wt% PVAc solution electrospun for 3 min at 20 kV with a 0.5 mL h⁻¹ flow rate and a distance of 220 cm. Next, an aluminum foil was folded to obtain vertical edges of 4 cm in height, which were then coated with the 14 wt% PAN solution electrospun almost parallel to the aluminum edges to create aligned fibers. PAN electrospinning was performed at 13 kV with a flow rate of 1 mL h⁻¹ for a total of 5 min and a spinning distance of 220 cm (from the charged bar to the flat plate, i.e., 216 cm from the tip of the aluminum edges). Then the fibrous mat was transferred from the aluminum onto the ITO substrates by heating in a benchtop oven at 80 °C for 3 min to dissolve the PVAc glue and to firmly attach the aligned PAN fibers to the ITO substrates.

Wrapping of pDR1M platforms around the PAN fibers was obtained by casting a drop of dispersed platforms in water directly onto the fiber mat and inducing rolling with a linear polarizer aligned with the fibers direction as described before. Imaging of the dried fibers was also performed as explained before.

Bending stress and strain calculations

The bending stress σ (circumferential stress σ_x) of pDR1M platforms was calculated according to Eq. (1), where E is the Young's modulus, ν the Poisson's ratio, ϵ the surface bending strain, t the film thickness, and R the bending radius^{62,63}

$$\sigma_x = \frac{E}{1 - \nu^2} \epsilon_x \text{ with } : \epsilon_x = \frac{t}{2R} \quad (1)$$

The bending strain ϵ of a thin film on either the inside (compressive strain) or outside (tensile strain) surface of a rolling platform was calculated according to Eq. (2), where t_f is the thickness of the film, t_s the thickness of the substrate (pDR1M), d the bending diameter, E_f the film Young's modulus, and E_s the substrate (pDR1M) Young's modulus³¹.

$$\epsilon = \frac{t_f + t_s}{d} \frac{1 + 2\frac{t_f}{t_s} + \frac{E_f}{E_s} \left(\frac{t_f}{t_s}\right)^2}{\left(1 + \frac{t_f}{t_s}\right) \left(1 + \frac{E_f t_f}{E_s t_s}\right)} \quad (2)$$

The materials characteristics described in Table 1 have been used for the calculations.

Neuronal culture and wrapping with pDR1M platforms

Materials. Glass coverslips (#0, Ø12 mm, Carolina, cat# 633009), ethanol 70% (EtOH 70%, Decon Labs 140 Proof, VWR, cat# 76212-358), 24 well plates (glass bottom, #1.5H, Cellvis, cat# P24-1.5H-N), Gibco Poly-D-Lysine (PDL, 0.1 mg mL⁻¹, ThermoFisher, cat# A3890401), Gibco B-27 Plus Neuronal Culture System (Neurobasal™ Plus Medium and B-27™

Table 1 | Parameters used to calculate the bending strain of thin films with Eq. 2

	pDR1M ²⁹	CNT ^{64,65}	Graphene ⁶⁶	h-BN ⁶⁷	Parylene-C ^{68,69}	MoS ₂ ⁷⁰	Ti ₃ C ₂ Ti _x ⁷¹	PEDOT:PSS ⁷²	Au ⁷³	Ti ^{74,75}	SiO ₂ ⁷⁶
Thickness t (nm)	150	1	0.33	0.33	30	0.7	1	25	30	40	20
Young's modulus E (GPa)	1	1000	1000	870	3.5	270	333	2	45	110	65
Strain at break ϵ_{\max} (%)	–	16	13	13	30	8	5	10	3	2	0.6

The values were obtained or approximated from the references listed next to each material.

Plus Supplement (50X), ThermoFisher, cat# A3653401), Gibco GlutaMAX™ I Supplement (400X, ThermoFisher, cat# 35050061), Gibco Gentamicin (antibiotic, 1000X, 10 mg mL⁻¹, ThermoFisher, cat# 15710064). All materials were used as received without further purification.

Equipment. Ultrasonic bath (Branson CPX2800H, VWR, cat# 89375-492), plasma asher (Diener Atto, 13.56 MHz/300 W, Diener Electronic, Ebhausen, Germany), Centrifuge (Sorvall ST 8R, Thermo Scientific, Waltham, MA USA), cell incubator (Heracell VIOS 160i CO₂ incubator, Thermo Scientific, Waltham, MA USA), bright-field and fluorescence microscope (Nikon ECLIPSE Ti inverted microscope, Lumencore SPECTRA X Light Engine, Hamamatsu C10600 ORCA-R² digital camera, and Nikon NIS Elements acquisition software).

The plating medium was aseptically prepared fresh by mixing the Neurobasal medium with 2% B-27 supplement (20 mL L⁻¹) and 0.25% GlutaMAX supplement to obtain a 0.5 mM concentration (2.5 mL L⁻¹). In comparison, the culture medium was prepared the same way but with the addition of 0.1% of Gentamicin antibiotic (1 mL L⁻¹). Culture media were kept at 4 °C for up to 2 weeks. Glass coverslips were immersed in EtOH 70%, sonicated for 10 min, and dried with a nitrogen gun before being sterilized with an oxygen plasma for 2 min at 200 W, 0.7 mbar. Then, the coverslips were transferred aseptically to a biosafety cabinet and inserted into the 24 well plates. Next, each coverslip was coated with 100 μ L of PDL for 2 h at room temperature, rinsed twice with 1 mL of MicroPure sterile-filtered water, and let air-dry with the plate lid open. At this point, the coverslips were ready to accommodate the cells. Dissociated primary hippocampal rat neurons (E18 Sprague Dawley) were purchased from TransnetYX Tissue (cat# SDEDHP, Cordova, TN USA). The cells were centrifuged with gentle acceleration for 1:30 min at 1100 rpm, redispersed in the plating medium at a concentration of 500'000 cells per mL, and seeded on the PDL-coated coverslips at a density of 22,000 cells per cm² (50 μ L of cells dispersion, i.e., ~25,000 cells per coverslip). After incubation at 37 °C for 45 min, 0.5 mL of warm culture medium was added to each well. The cells were kept in the cell incubator, and 40–50% of their medium was exchanged with fresh warm culture medium every 3–4 days.

pDR1M platforms reserved for cell experiments were etched as described before and considered sterile immediately after the plasma. Hence, the substrates were transferred aseptically to a biosafety cabinet and harvested in 15 μ L of cell medium from 7 days or older cultures. Then, the platforms were directly dispersed onto the cells and incubated with the cultures for 2 days before wrapping. Wrapping and imaging of pDR1M platforms around neuronal processes were obtained with an inverted light microscope and rolling induced with 555 nm illumination at 8 mW mm⁻² for 6 s.

Cell viability assays

Materials. MTT Cell Viability Assay Kit (Biotium, cat# 30006), Dimethylsulfoxide (DMSO, ATCC, cat# 4-X), Invitrogen™ Neurite Outgrowth Staining Kit (Cell Viability Indicator 1000X and Cell Membrane Stain 1000X, ThermoFisher, cat# A15001), Phosphate Buffered Saline (PBS, pH 7.4, sterile-filtered, Sigma-Aldrich, cat# 806552), Hanks' Balanced Salt solution (HBSS, with calcium and magnesium, without phenol red, Sigma-Aldrich, cat# 55037 C).

Equipment. Microplate reader (Synergy 2, multi-detection, Gen5 acquisition software, Biotek, Winooski, VT USA).

The MTT cell metabolic activity assays were performed according to the supplier protocol. Briefly, the neurons were plated directly into 96 well plates following the previous procedure and with 200 μ L of culture medium. For all the conditions and controls described in the results section, neurons were cultured for 16 days total, while only the timing where the platforms were introduced in the medium changed. At the end of the incubation periods with the various conditions described in the results section, the medium of each well was brought to 100 μ L and supplied with 10 μ L of the MTT solution, mixed gently, and incubated at 37 °C for 4 hours. Then, 200 μ L of DMSO were added to each well, and the entire volume was pipetted up and down several times to dissolve the formazan salt and homogenize the content. Finally, absorbance signals were measured with a spectrophotometric microplate reader for each well at 570 nm and 630 nm for background absorbance. Normalized absorbance values (plotted in Fig. 5C-i) were obtained by subtracting the background absorbance from signal absorbance at 570 nm. The cell viability was calculated according to Eq. (3), where A_{c+p} is the absorbance value for the cells with the platforms, A_{m+p} for the medium with the platforms, A_c for the cells, A_m for the medium, and A^{570} and A^{630} are the signal and the background values, respectively.

$$viability = \frac{(A_{c+p}^{570} - A_{c+p}^{630}) - (A_{m+p}^{570} - A_{m+p}^{630})}{(A_c^{570} - A_c^{630}) - (A_m^{570} - A_m^{630})} \times 100 \quad (3)$$

The cell viability and neurite outgrowth staining was performed according to the supplier protocol. Briefly, the neurons cultured on 12 mm coverslips were rinsed with warm PBS once, immersed in a solution of HBSS mixed with the provided Cell Membrane Stain (1 μ L mL⁻¹) and Cell Viability Indicator (1 μ L mL⁻¹), and incubated at 37 °C for 20 min. Then, the cells were rinsed once with PBS and immersed in a solution of HBSS mixed with the provided Background Suppression Dye (10 μ L mL⁻¹) to be imaged with an inverted fluorescence microscope and a FITC filter set for the cell viability indicator and TRITC for the cell membrane staining. Lookup table is kept linear and covers the full range of data.

Cell preparation for SEM imaging

Materials. Sodium Cacodylate (trihydrate, Electron Microscopy Sciences, cat# 12310), Glutaraldehyde (GA, 10%, EM grade, Electron Microscopy Sciences, cat# 16120), Paraformaldehyde (PFA, 16%, EM grade, Electron Microscopy Sciences, cat# 15710), Osmium Tetroxide (OsO₄, Electron Microscopy Sciences, cat# 19110), Ethanol (Koptec 200 PROOF, Decon Labs, cat# V1001), Tetramethyl Silane (TMS, 99%, Acros Fisher Scientific, cat# 10338770). All materials were used as received without further purification.

Equipment. Gold sputter (Desk V, Denton Vacuum, Moorestown, NJ USA).

The 0.2 M and 0.1 M cacodylate buffers were prepared by dissolving 4.28 g and 2.14 g, respectively, of sodium cacodylate in 100 mL UltraPure water. The fixative solution consisted of 2.5% GA and 2% PFA in 0.1 M cacodylate buffer and was prepared fresh (starting with 0.2 M buffer and diluting with water to obtain 0.1 M final). To fix the cells on the 12 mm

Table 2 | Intracellular solution composition

Component	Concentration [mM]
Potassium gluconate	125
NaCl	8
CaCl ₂	0.1
MgCl ₂	0.6
EGTA	1
HEPES	10
Mg-ATP	4
Na-GTP	0.4

coverslips, the medium was removed from the well, and the cells were rinsed once with PBS and immersed in the fixative solution for 1 h at 4 °C. After that, the cells were rinsed three times with 0.1 M cacodylate buffer for 5 min and kept in the buffer overnight at 4 °C. Then, post-fixation with OsO₄ was obtained by exposing the cells to a 1% OsO₄ solution in 0.1 M cacodylate buffer for 30 min at 4 °C. Next, the cells were rinsed four times with UltraPure water for 10 minutes to remove all fixative and salts residues, and dehydration was achieved by exchanging the water to 35%, 45%, 50%, 65%, 70%, 85%, 95%, and 100% ethanol for 5 min each, shaking delicately and frequently. Then, exchange to TMS was performed by immersing the cells in a 50% TMS and ethanol solution for 15 minutes, then 80% again for 15 minutes, and lastly twice in 100% TMS for 5 min. Finally, the TMS was let evaporate overnight at room temperature, and the dried cells were sputtered at 50 mA for 120 s with a conductive gold coating (~10 nm) and imaged at the SEM as described before.

Patch-clamping

Materials. Glass capillaries with filament (World precision instruments, cat# 1B150F4), microloaders (VWR, Cat# 89009-310), potassium gluconate (Sigma-Aldrich, cat# P1847), sodium chloride (NaCl, Sigma-Aldrich, cat# S9888-1KG), calcium chloride (CaCl₂, Sigma-Aldrich, cat# C4901-100G), magnesium chloride (MgCl₂, Sigma-Aldrich, cat# M8266-100G), ethylene glycol tetraacetic acid (EGTA, Sigma-Aldrich, cat#E0396-10G), 4-(2-Hydroxyethyl)piperazine-1-ethanesulfonic acid (HEPES, Sigma-Aldrich, cat# H3375-500G), adenosine 5'-triphosphate magnesium salt (Mg-ATP, Sigma-Aldrich, cat# A9187-1G), guanosine 5'-triphosphate sodium salt hydrate (Na-GTP, Sigma-Aldrich, cat# G8877-250MG), sucrose (Sigma-Aldrich, cat# S0389-1KG), and potassium hydroxide (KOH, Sigma-Aldrich, cat #P1767-250G).

Equipment. Inverted microscope (Nikon, Ti2E), patch-clamp amplifier (Molecular Devices Axon Multiclamp 700B), digitizer (Molecular Devices Axon Digidata 1550B), motorized micromanipulator (Scientifica, PatchStar), motorized platform (Scientifica, Inverted motorized movable top plate), and micropipette puller (Sutter Instrument, P-97).

The patch-clamp intracellular solution was prepared following Table 2. After adding the listed salts in sterile de-ionized water to reach the desired concentration, the pH was adjusted to 7.3 with KOH (5 M) and the osmolarity to 295–300 mOsm with sucrose. The intracellular solution was aliquoted in 1 ml tubes and stored at –20 °C. Patch-clamp micropipettes were freshly pulled and filled with the intracellular solution using microloaders just before the experiment (pipette resistance ~5 MΩ). Whole-cell current clamp experiments were performed on primary rat hippocampal neurons in their medium.

Immunocytochemistry

Materials. Phosphate Buffered Saline (PBS, pH 7.4, sterile-filtered, Sigma-Aldrich, cat# 806552), Paraformaldehyde 32% solution (PFA, diluted to 4% in PBS, EM grade, Electron Microscopy Sciences cat# 15714), Triton X-100 (Sigma-Aldrich, cat# T8787), normal goat serum

(Abcam, cat# AB138478), rabbit anti-alpha tubulin antibody (primary antibody, Abcam, cat# AB4074), Alexa Fluor 488 goat anti-rabbit IgG (secondary antibody, H + L, Invitrogen, cat# A11008), ProLong Glass Antifade Mountant with NucBlue Stain (ThermoFisher, cat# P36983).

Equipment. Fluorescence microscope (Nikon ECLIPSE Ti inverted microscope, Lumencore SPECTRA X Light Engine, Hamamatsu C10600 ORCA-R² digital camera, and Nikon NIS Elements acquisition software).

16-day-old cells cultured with and without platforms were washed with PBS and fixed with PFA 4% before permeabilization with 0.25% Triton X-100 in PBS for 10 min. Blocking was performed with 0.25% Triton X-100 and 5% normal goat serum in PBS for 45 min. The cells were then incubated with 0.25% Triton X-100, 5% normal goat serum, and 2 μg mL⁻¹ primary antibody in PBS overnight at 4 °C. After washing the cells with 0.1% Triton X-100 in PBS, incubation with 0.25% Triton X-100, 5% normal goat serum, and 2 μg mL⁻¹ secondary antibody in PBS was performed at room temperature for 1 h. Finally, the cells were washed again with 0.1% Triton X-100 in PBS, mounted on a coverslip with mountant including DAPI nuclei staining for 24 h at room temperature, and imaged with an inverted fluorescence microscope. Lookup table is kept linear and covers the full range of data.

Reporting summary

Further information on research design is available in the Nature Portfolio Reporting Summary linked to this article.

Data availability

All materials are commercially available. All data needed to support the findings of this study are available in the manuscript, supplementary information, and in FIGSHARE repository <https://doi.org/10.6084/m9.figshare.27128991>, [27128985](https://doi.org/10.6084/m9.figshare.27128985), and [27128979](https://doi.org/10.6084/m9.figshare.27128979).

Received: 11 August 2024; Accepted: 18 October 2024;

Published online: 30 October 2024

References

- Tahirovic, S. & Bradke, F. Neuronal polarity. *Cold Spring Harb. Perspect. Biol.* **1**, a001644 (2009).
- Batish, M., Van Den Bogaard, P., Kramer, F. R. & Tyagi, S. Neuronal mRNAs travel singly into dendrites. *Proc. Natl Acad. Sci. USA* **109**, 4645–4650 (2012).
- Trimmer, J. S. Subcellular localization of K⁺ channels in mammalian brain neurons: remarkable precision in the midst of extraordinary complexity. *Neuron* **85**, 238–256 (2015).
- Winckler, B., Forscher, P. & Mellman, I. A diffusion barrier maintains distribution of membrane proteins in polarized neurons. *Nature* **397**, 698–701 (1999).
- Aiken, J. & Holzbaur, E. L. F. Cytoskeletal regulation guides neuronal trafficking to effectively supply the synapse. *Curr. Biol.* **31**, R633–R650 (2021).
- Leterrier, C. & Leterrier, X. C. The axon initial segment: an updated viewpoint. *J. Neurosci.* **38**, 2135–2145 (2018).
- van Bergeijk, P., Hoogenraad, C. C. & Kapitein, L. C. Right time, right place: probing the functions of organelle positioning. *Trends Cell Biol.* **26**, 121–134 (2016).
- van Oostrum, M. et al. Surfaceome dynamics reveal proteostasis-independent reorganization of neuronal surface proteins during development and synaptic plasticity. *Nat. Commun.* **11**, 1–16 (2020).
- Liang, E., Shi, J. & Tian, B. Freestanding nanomaterials for subcellular neuronal interfaces. *iScience* **25**, 103534 (2022).
- Garcia-Etxarri, A. & Yuste, R. Time for NanoNeuro. *Nat. Methods* **18**, 1287–1293 (2021).
- Chen, R., Canales, A. & Anikeeva, P. Neural recording and modulation technologies. *Nat. Rev. Mater.* **2**, 1–16 (2017).

12. Rivnay, J., Wang, H., Fenno, L., Deisseroth, K. & Malliaras, G. G. Next-generation probes, particles, and proteins for neural interfacing. *Sci. Adv.* **3**, e1601649 (2017).
13. Guo, Z., Richardson, J. J., Kong, B. & Liang, K. Nanobiohybrids: materials approaches for bioaugmentation. *Sci. Adv.* **6**, 330–348 (2020).
14. Reich, D. S., Lucchinetti, C. F. & Calabresi, P. A. Multiple Sclerosis. *N. Engl. J. Med.* **378**, 169–180 (2018).
15. Liewald, D., Miller, R., Logothetis, N., Wagner, H. J. & Schüz, A. Distribution of axon diameters in cortical white matter: an electron-microscopic study on three human brains and a macaque. *Biol. Cyber.* **108**, 541–557 (2014).
16. Ledesma, H. A. et al. An atlas of nano-enabled neural interfaces. *Nat. Nanotechnol.* **14**, 645–657 (2019).
17. Airaghi Leccardi, M. J. I. & Ghezzi, D. Organic electronics for neuroprosthetics. *Health. Technol. Lett.* **7**, 52–57 (2020).
18. Probst, C. et al. Athermal azobenzene-based nanoimprint lithography. *Adv. Mater.* **28**, 2624–2628 (2016).
19. Yu, Y., Nakano, M. & Ikeda, T. Directed bending of a polymer film by light. *Nature* **425**, 145 (2003).
20. Pang, X., Lv, J., Zhu, C., Qin, L. & Yu, Y. Photodeformable azobenzene-containing liquid crystal polymers and soft actuators. *Adv. Mater.* **31**, 1904224 (2019).
21. Maiti, S. et al. Distribution and orientation of nerve fibers and myelin assembly in a brain section retrieved by small-angle neutron scattering. *Sci. Rep.* **11**, 1–14 (2021).
22. Gibbons, W. M., Shannon, P. J., Sun, S. T. & Swetlin, B. J. Surface-mediated alignment of nematic liquid crystals with polarized laser light. *Nature* **351**, 49–50 (1991).
23. Yun, J. H., Li, C., Kim, S. & Cho, M. Comparing photoactuation of an azobenzene-doped nematic liquid crystal polymer through its activation mechanism: trans-cis-trans reorientation and photoisomerization. *J. Phys. Chem. C.* **122**, 6310–6317 (2018).
24. Yu, Y. & Ikeda, T. Alignment modulation of azobenzene-containing liquid crystal systems by photochemical reactions. *J. Photochem. Photobiol. C Photochem. Rev.* **5**, 247–265 (2004).
25. Vohra, V. & Anzai, T. Molecular orientation of conjugated polymer chains in nanostructures and thin films: Review of processes and application to optoelectronics. *J. Nanomater.* **2017**, 3624750 (2017).
26. Liu, J., Yu, X., Xue, L. & Han, Y. Morphology control of polymer thin Films. in *Polymer Morphology: Principles, Characterization, and Processing* (ed Guo, Q.) 299–316 (John Wiley & Sons, Ltd, 2016). <https://doi.org/10.1002/9781118892756.CH16>.
27. Del Pozo, M., Sol, J. A. H. P., Schenning, A. P. H. J. & Debije, M. G. 4D printing of liquid crystals: what's right for me? *Adv. Mater.* **34**, 2104390 (2021).
28. Weis, P., Tian, W. & Wu, S. Photoinduced liquefaction of azobenzene-containing polymers. *Chem. Eur. J.* **24**, 6494–6505 (2018).
29. Kim, K.-H. & Jeong, Y.-C. Nanoindentation study of optically patterned surface relief grating of azobenzene polymers. *Opt. Express* **24**, 25242–25249 (2016).
30. Madeshwaran, S. R., Kwon, J. K. & Cho, J. W. Functionalized multi-walled carbon nanotubes with hyperbranched aromatic polyamide for poly(methyl methacrylate) composites. *Fibers Polym.* **14**, 182–187 (2013).
31. Leterrier, Y. Mechanics of curvature and strain in flexible organic electronic devices. In *Handbook of Flexible Organic Electronics: Materials, Manufacturing and Applications* 3–36 (Woodhead Publishing, 2015) <https://doi.org/10.1016/B978-1-78242-035-4.00001-4>.
32. Yu, L., Ruzsinszky, A. & Perdew, J. P. Bending two-dimensional materials to control charge localization and fermi-level shift. *Nano Lett.* **16**, 2444–2449 (2016).
33. Yu, J. et al. Designing the bending stiffness of 2D material heterostructures. *Adv. Mater.* **33**, 2007269 (2021).
34. Yang, S., Chen, Y. & Jiang, C. Strain engineering of two-dimensional materials: methods, properties, and applications. *InfoMat* **3**, 397–420 (2021).
35. Vaquero, S. et al. Conjugated polymers for the optical control of the electrical activity of living cells. *J. Mater. Chem. B* **4**, 5272–5283 (2016).
36. Vagni, P. et al. POLYRETINA restores light responses in vivo in blind Göttingen minipigs. *Nat. Commun.* **13**, 1–14 (2022).
37. Airaghi Leccardi, M. J. I. et al. Photovoltaic organic interface for neuronal stimulation in the near-infrared. *Commun. Mater.* **1**, 1–13 (2020).
38. Lanzani, G., Antognazza, M. R., Martino, N., Ghezzi, D. & Benfenati, F. Controlling cell functions by light. In *International IEEE/EMBS Conference on Neural Engineering, NER* vols 2015–July 603–606 (IEEE Computer Society, 2015).
39. Efos, A. L. et al. Evaluating the potential of using quantum dots for monitoring electrical signals in neurons. *Nat. Nanotechnol.* **13**, 278–288 (2018).
40. Habib, A. et al. Electro-plasmonic nanoantenna: a nonfluorescent optical probe for ultrasensitive label-free detection of electrophysiological signals. *Sci. Adv.* **5**, aav9786 (2019).
41. Carnicer-Lombarte, A., Chen, S. T., Malliaras, G. G. & Barone, D. G. Foreign body reaction to implanted biomaterials and its impact in nerve neuroprosthetics. *Front. Bioeng. Biotechnol.* **9**, 271 (2021).
42. Shemesh, O. A. et al. Temporally precise single-cell-resolution optogenetics. *Nat. Neurosci.* **20**, 1796–1806 (2017).
43. Rijnbeek, E. H., Eleveld, N. & Olthuis, W. Update on peripheral nerve electrodes for closed-loop neuroprosthetics. *Front. Neurosci.* **12**, 350 (2018).
44. Maya-Vetencourt, J. F. et al. Subretinally injected semiconducting polymer nanoparticles rescue vision in a rat model of retinal dystrophy. *Nat. Nanotechnol.* **15**, 698–708 (2020).
45. Rand, D. et al. Direct electrical neurostimulation with organic pigment photocapacitors. *Adv. Mater.* **30**, 1707292 (2018).
46. Zimmerman, J. F. & Tian, B. Non-genetic optical methods for measuring and modulating neuronal response. *ACS Nano* **12**, 4086 (2018).
47. Desbiolles, B. X. E., Coulon, E., de Bertsch, A., Rohr, S. & Renaud, P. Intracellular recording of cardiomyocyte action potentials with nanopatterned volcano-shaped microelectrode arrays. *Nano Lett.* **19**, 6173–6181 (2019).
48. Airaghi Leccardi, M. J. I., Vagni, P. & Ghezzi, D. Multilayer 3D electrodes for neural implants. *J. Neural Eng.* **16**, 026013 (2019).
49. Carvalho-de-Souza, J. L., Pinto, B. I., Pepperberg, D. R. & Bezanilla, F. Optocapacitive generation of action potentials by microsecond laser pulses of nanojoule energy. *Biophys. J.* **114**, 283 (2018).
50. Kaisti, M. Detection principles of biological and chemical FET sensors. *Biosens. Bioelectron.* **98**, 437–448 (2017).
51. Kajale, S. N., Yadav, S., Cai, Y., Joy, B. & Sarkar, D. 2D material based field effect transistors and nanoelectromechanical systems for sensing applications. *iScience* **24**, 103513 (2021).
52. Gregurec, D. et al. Magnetic vortex nanodiscs enable remote magnetomechanical neural stimulation. *ACS Nano* **14**, 8036–8045 (2020).
53. Pollerberg, G. E., Thelen, K., Theiss, M. O. & Hochlehnert, B. C. The role of cell adhesion molecules for navigating axons: Density matters. *Mech. Dev.* **130**, 359–372 (2013).
54. Manoukian, O. S. et al. Biomaterials for tissue engineering and regenerative medicine. *Encycl. Biomed. Eng.* **1–3**, 462–482 (2019).
55. Ratner, B. D. Polymeric implants. *Polym. Sci. Compr. Ref.* **1–10**, 397–411 (2012).
56. Lee, K. M. & White, T. J. Photomechanical response of composite structures built from azobenzene liquid crystal polymer networks. *Polymers* **3**, 1447–1457 (2011).
57. Kozielski, K. L. et al. Nonresonant powering of injectable nanoelectrodes enables wireless deep brain stimulation in freely moving mice. *Sci. Adv.* **7**, 4189–4202 (2021).

58. Shen, Z., Chen, F., Zhu, X., Yong, K. T. & Gu, G. Stimuli-responsive functional materials for soft robotics. *J. Mater. Chem. B* **8**, 8972–8991 (2020).
59. Liu, J., Gao, Y., Lee, Y. J. & Yang, S. Responsive and foldable soft materials. *Trends Chem.* **2**, 107–122 (2020).
60. Lee, Y. H. et al. Recent advances in organic sensors for health self-monitoring systems. *J. Mater. Chem. C. Mater.* **6**, 8569–8612 (2018).
61. Abbasi Kajani, A., Haghjooy Javanmard, S., Asadnia, M. & Razmjou, A. Recent Advances in Nanomaterials Development for Nanomedicine and Cancer. *ACS Appl Bio Mater.* **4**, 5908–5925 (2021).
62. Patel, S. K., Lal, R. K., Dwivedi, J. P. & Singh, V. P. Springback analysis in sheet metal forming using modified Ludwik stress-strain relation. *ISRN Mech. Eng.* **2013**, 640958 (2013).
63. Kollár, L. P. & Tarján, G. Plates. In *Mechanics of Civil Engineering Structures* 365–428 (Woodhead Publishing, 2021) <https://doi.org/10.1016/B978-0-12-820321-7.00010-1>.
64. Li, C. & Chou, T. W. A structural mechanics approach for the analysis of carbon nanotubes. *Int J. Solids Struct.* **40**, 2487–2499 (2003).
65. Wernik, J. M. & Meguid, S. A. Atomistic-based continuum modeling of the nonlinear behavior of carbon nanotubes. *Acta Mech.* **212**, 167–179 (2009).
66. Zhang, Y. Y. & Gu, Y. T. Mechanical properties of graphene: effects of layer number, temperature and isotope. *Comput Mater. Sci.* **71**, 197–200 (2013).
67. Falin, A. et al. Mechanical properties of atomically thin boron nitride and the role of interlayer interactions. *Nat. Commun.* **8**, 1–9 (2017).
68. Rapp, B. E., Voigt, A., Dirschka, M. & Länge, K. Deposition of ultrathin parylene C films in the range of 18 nm to 142 nm: Controlling the layer thickness and assessing the closeness of the deposited films. *Thin Solid Films* **520**, 4884–4888 (2012).
69. Hassler, C., Von Metzen, R. P., Ruther, P. & Stieglitz, T. Characterization of parylene C as an encapsulation material for implanted neural prostheses. *J. Biomed. Mater. Res B Appl Biomater.* **93B**, 266–274 (2010).
70. Bertolazzi, S., Brivio, J. & Kis, A. Stretching and breaking of ultrathin MoS₂. *ACS Nano* **5**, 9703–9709 (2011).
71. Lipatov, A. et al. Elastic properties of 2D Ti₃C₂T_x MXene monolayers and bilayers. *Sci. Adv.* **4**, 6 (2018).
72. Lipomi, D. J. et al. Electronic properties of transparent conductive films of PEDOT:PSS on stretchable substrates. *Chem. Mater.* **24**, 373–382 (2012).
73. Kim, J. H. et al. Tensile testing of ultra-thin films on water surface. *Nat. Commun.* **4**, 1–6 (2013).
74. Cordill, M. J. & Taylor, A. A. Thickness effect on the fracture and delamination of titanium films. *Thin Solid Films* **589**, 209–214 (2015).
75. Ogawa, H. et al. Tensile testing of microfabricated thin films. *Microsyst. Technol.* **117**, 121 (1997).
76. Sharpe, W. N. et al. Strain measurements of silicon dioxide microspecimens by digital imaging processing. *Exp. Mech.* **47**, 649–658 (2007).

Acknowledgements

We thank Yubin Cai for 3D printing the custom-made molding system. Fabrication and electron microscopy imaging were performed at MIT.nano cleanroom and characterization facilities. Cells preparation for electron microscopy was performed with equipment and support from the MIT Koch Institute, Nanotechnology Materials Core. Specifically, we thank Abigail Lytton-Jean, David Mankus, and Margaret Bisher from the MIT Koch Institute Nanotechnology Materials Core for the fruitful discussion and inputs.

Confocal microscopy was performed with equipment at the MIT Koch Institute Microscopy Facility. Finally, we also thank the MIT Rutledge Research Group, which supplied us with the synthetic fibers. This work was supported by the Swiss National Science Foundation (project number P2ELP2_191218) and the American National Institutes of Health Brain Initiative (NIH grant 1-R21-EY034283-01).

Author contributions

M.J.I.A.L. conceived the project, designed the experiments, fabricated the structures, performed the imaging, characterization, experiments, data analysis, and stress/strain calculations, and hypothesized the photoinduced mechanisms. B.X.E.D. performed the UV-Vis spectroscopy, designed the custom-made molding system, helped with cell culture, experimental design, patch-clamping, imaging, and provided essential inputs. M.J.I.A.L. and A.Y.H. cultured the cells and performed the viability imaging. B.C.J. cultured the cells. C.S. produced the synthetic fibers. D.S. supervised the project, made key contributions, and validated data analysis. M.J.I.A.L. wrote the manuscript and prepared the figures with input from all the coauthors.

Competing interests

The authors M.J.I. Airaghi Leccardi and D. Sarkar have filed a provisional patent application related to the work reported in this manuscript. All other authors declare no competing interests

Additional information

Supplementary information The online version contains supplementary material available at <https://doi.org/10.1038/s42004-024-01335-8>.

Correspondence and requests for materials should be addressed to Deblina Sarkar.

Peer review information *Communications Chemistry* thanks the anonymous reviewers for their contribution to the peer review of this work.

Reprints and permissions information is available at <http://www.nature.com/reprints>

Publisher's note Springer Nature remains neutral with regard to jurisdictional claims in published maps and institutional affiliations.

Open Access This article is licensed under a Creative Commons Attribution-NonCommercial-NoDerivatives 4.0 International License, which permits any non-commercial use, sharing, distribution and reproduction in any medium or format, as long as you give appropriate credit to the original author(s) and the source, provide a link to the Creative Commons licence, and indicate if you modified the licensed material. You do not have permission under this licence to share adapted material derived from this article or parts of it. The images or other third party material in this article are included in the article's Creative Commons licence, unless indicated otherwise in a credit line to the material. If material is not included in the article's Creative Commons licence and your intended use is not permitted by statutory regulation or exceeds the permitted use, you will need to obtain permission directly from the copyright holder. To view a copy of this licence, visit <http://creativecommons.org/licenses/by-nc-nd/4.0/>.

© The Author(s) 2024